All-optical scanhead for ultrasound and photoacoustic dual-modality imaging

Bao-Yu Hsieh,[1] Sung-Liang Chen,[2] Tao Ling,[2] L. Jay Guo,[2] and Pai-Chi Li[1,3,*]

[1]*Graduate Institute of Biomedical Electronics and Bioinformatics, National Taiwan University, Taipei, Taiwan*
[2]*Department of Electrical Engineering and Computer Science, University of Michigan, Ann Arbor, Michigan, USA*
[3]*Department of Electrical Engineering, National Taiwan University, Taipei, Taiwan*
**paichi@cc.ee.ntu.edu.tw*

Abstract: We propose a new scanhead design for combined ultrasound (US)/photoacoustic (PA) imaging that can be applied to dual-modality microscopy and biomedical imaging. Both imaging modalities employ the optical generation and detection of acoustic waves. The scanhead consists of an optical fiber with an axicon tip for excitation, and a microring for acoustic detection. No conventional piezoelectric device is needed, and the cost of the design makes it suitable for one-time, disposable use. Furthermore, a single laser pulse is employed to generate both US and PA signals. A subband imaging method can be applied to the receiver to enhance the contrast between the US and PA signals. Phantom data demonstrate the feasibility of this approach.

OCIS codes: (110.7170) Ultrasound; (170.5120) Photoacoustic imaging.

References and links

1. B. W. Drinkwater and P. D. Wilcox, "Ultrasonic arrays for non-destructive evaluation: a review," NDT Int. **39**(7), 525–541 (2006).
2. S. J. Song, H. J. Shin, and Y. H. Jang, "Development of an ultrasonic phased array system for nondestructive tests of nuclear power plant components," Nucl. Eng. Des. **214**(1–2), 151–161 (2002).
3. G. Grégoire, V. Tournat, D. Mounier, and V. E. Gusev, "Nonlinear photothermal and photoacoustic processes for crack detection," Eur. Phys. J. Spec. Top. **153**(1), 313–315 (2008).
4. S. Sethuraman, S. R. Aglyamov, J. H. Amirian, R. W. Smalling, and S. Y. Emelianov, "Intravascular photoacoustic imaging using an IVUS imaging catheter," IEEE Trans. Ultrason. Ferroelectr. Freq. Control **54**(5), 978–986 (2007).
5. W. Wei, X. Li, Q. Zhou, K. K. Shung, and Z. Chen, "Integrated ultrasound and photoacoustic probe for co-registered intravascular imaging," J. Biomed. Opt. **16**(10), 106001 (2011).
6. S. Mallidi, A. B. Karpiouk, S. R. Aglyamov, S. Sethuraman, and S. Y. Emelianov, "Measurement of blood perfusion using photoacoustic, ultrasound, and strain imaging," Proc. SPIE **6437**, 643707, 643707-9 (2007).
7. K. Homan, J. Shah, S. Gomez, H. Gensler, A. B. Karpiouk, L. Brannon-Peppas, and S. Y. Emelianov, "Combined ultrasound and photoacoustic imaging of pancreatic cancer using nanocage contrast agents," Proc. SPIE **7177**, 71771M, 71771M-6 (2009).
8. S. Hu and L. V. Wang, "Photoacoustic imaging and characterization of the microvasculature," J. Biomed. Opt. **15**(1), 011101 (2010).
9. J. Shah, S. Park, S. R. Aglyamov, T. Larson, L. Ma, K. Sokolov, K. Johnston, T. Milner, and S. Y. Emelianov, "Photoacoustic imaging and temperature measurement for photothermal cancer therapy," J. Biomed. Opt. **13**(3), 034024 (2008).
10. S. Kim, Y. S. Chen, G. P. Luke, M. Mehrmohammadi, J. R. Cook, and S. Y. Emelianov, "Ultrasound and photoacoustic image-guided photothermal therapy using silica-coated gold nanorods: in-vivo study," Proc. of IEEE IUS, 233–236 (2010).
11. J. M. Cannata, J. A. Williams, Qifa Zhou, T. A. Ritter, and K. K. Shung, "Development of a 35-MHz piezo-composite ultrasound array for medical imaging," IEEE Trans. Ultrason. Ferroelectr. Freq. Control **53**(1), 224–236 (2006).
12. T. Buma, M. Spisar, and M. O'Donnell, "High-frequency ultrasound array element using thermoelastic expansion in an elastomeric film," Appl. Phys. Lett. **79**(4), 548–550 (2001).
13. Y. Hou, J. S. Kim, S. Ashkenazi, M. O'Donnell, and L. J. Guo, "Optical generation of high frequency ultrasound using two-dimensional gold nanostructure," Appl. Phys. Lett. **89**(9), 093901 (2006).
14. Y. Hou, J. S. Kim, S. Ashkenazi, S. W. Huang, L. J. Guo, and M. O'Donnell, "Broadband all-optical ultrasound transducers," Appl. Phys. Lett. **91**(7), 073507 (2007).
15. K. Passler, R. Nuster, S. Gratt, P. Burgholzer, and G. Paltauf, "Laser-generation of ultrasonic X-waves using axicon transducers," Appl. Phys. Lett. **94**(6), 064108 (2009).

#158690 - $15.00 USD Received 23 Nov 2011; revised 28 Dec 2011; accepted 28 Dec 2011; published 10 Jan 2012

16. S. Resink, J. Jose, R. G. H. Willemink, C. H. Slump, W. Steenbergen, T. G. van Leeuwen, and S. Manohar, "Multiple passive element enriched photoacoustic computed tomography," Opt. Lett. **36**(15), 2809–2811 (2011).
17. J. D. Hamilton, T. Buma, M. Spisar, and M. O'Donnell, "High frequency optoacoustic arrays using etalon detection," IEEE Trans. Ultrason. Ferroelectr. Freq. Control **47**(1), 160–169 (2000).
18. P. C. Beard and T. N. Mills, "A 2D optical ultrasound array using a polymer film sensing interferometer," Proc. of IEEE IUS, 1183–1186 (2000).
19. E. Zhang, J. Laufer, and P. C. Beard, "Backward-mode multiwavelength photoacoustic scanner using a planar Fabry-Perot polymer film ultrasound sensor for high-resolution three-dimensional imaging of biological tissues," Appl. Opt. **47**(4), 561–577 (2008).
20. H. Tsuda, K. Kumakura, and S. Ogihara, "Ultrasonic sensitivity of strain-insensitive fiber Bragg grating sensors and evaluation of ultrasound-induced strain," Sensors **10**(12), 11248–11258 (2010).
21. V. Wilkens, "Characterization of an optical multilayer hydrophone with constant frequency response in the range from 1 to 75 MHz," J. Acoust. Soc. Am. **113**(3), 1431–1438 (2003).
22. R. Nuster, M. Holotta, C. Kremser, H. Grossauer, P. Burgholzer, and G. Paltauf, "Photoacoustic microtomography using optical interferometric detection," J. Biomed. Opt. **15**(2), 021307 (2010).
23. C. Y. Chao, S. Ashkenazi, S. W. Huang, M. O'Donnell, and L. J. Guo, "High-frequency ultrasound sensors using polymer microring resonators," IEEE Trans. Ultrason. Ferroelectr. Freq. Control **54**(5), 957–965 (2007).
24. S. W. Huang, S. L. Chen, T. Ling, A. Maxwell, M. O'Donnell, L. J. Guo, and S. Ashkenazi, "Low-noise wideband ultrasound detection using polymer microring resonators," Appl. Phys. Lett. **92**(19), 193509 (2008).
25. P. C. Li, C. W. Wei, and Y. L. Sheu, "Subband photoacoustic imaging for contrast improvement," Opt. Express **16**(25), 20215–20226 (2008).
26. M. Xu, Y. Xu, and L. V. Wang, "Time-domain reconstruction algorithms and numerical simulations for thermoacoustic tomography in various geometries," IEEE Trans. Biomed. Eng. **50**(9), 1086–1099 (2003).

1. Introduction

Ultrasound (US) imaging based on acoustic scattering and reflection can provide structural details of objects of interest, while photoacoustic (PA) imaging forms an image based on the optical absorption of pulsed laser light, where the absorbed laser energy leads to thermal expansion and the subsequent generation of acoustic waves. The similarity in the receivers has led to combined US and PA imaging as a dual-modality approach, which has been shown to be an efficient tool for nondestructive testing [1–3] and biomedical applications such as the detection of atherosclerotic plaques by intravascular imaging [4, 5], measurements of tumor blood perfusion [6–8], and for guiding and monitoring photothermal therapy [9, 10].

Conventional systems generate and detect US using transducers constructed from piezoelectric materials. High-frequency arrays are essential to achieving high resolution and high-frame-rate imaging. However, such arrays are difficult to fabricate using conventional piezoelectric materials due to the challenges of producing small elements, making tiny electrical connections, and the crosstalk among elements [11]. Optical generation and detection of ultrasound have potential to overcome these problems.

The optical generation of US is a promising alternative to the use of piezoelectricity for high-frequency arrays. The most common mechanism is based on the PA effect [12–14], whereby the material absorbs laser energy, undergoes thermal expansion, and thereby generates a broadband acoustic signal. It has been used as the acoustic source in pulse-echo US imaging [14–16]. Moreover, this technique has the potential to realize high-density transmitting arrays for high-frequency and high-frame-rate imaging since a micron-scale laser beam width can define a transducer element.

On the other hand, US has been optically detected using devices such as etalons [17–19], fiber gratings [20], dielectric multilayer interference filters [21], Mach-Zehnder interferometer [22], and polymer microring resonators [23, 24] for several decades. A polymer microring resonator is one type of optically based US sensor. It consists of an input/output bus waveguide and a coupled polystyrene ring waveguide. The ring waveguide is deformed by the incoming acoustic wave, which induces a corresponding change in the effective refractive index, resulting in a shift of the resonant wavelength. The acoustic waveform can be recovered by detecting the optical output intensity of the bus waveguide at a fixed laser wavelength. The microring device has several advantages, including being small (10–100 μm) and having a wide detection bandwidth (from DC to over 90 MHz at –3 dB), adequate SNR (noise-equivalent pressure = 0.23 kPa over 1–75 MHz), and no requirement for complicated back-end circuitry [23]. These characteristics make it an excellent candidate for high-

#158690 - $15.00 USD Received 23 Nov 2011; revised 28 Dec 2011; accepted 28 Dec 2011; published 10 Jan 2012

frequency receiving arrays. Moreover, the polymer microring resonator can be conveniently fabricated using a nanoimprinting technique, which makes mass production possible.

In this study we combined these optical-based techniques to develop a single-element all-optical integrated US/PA imaging scanhead. Images of a wire phantom and a grid phantom were acquired to demonstrate the feasibility of the all-optical scanhead and characterize its performance in US and PA imaging. In addition, a subband imaging technique can be used to separate the PA-based US and PA signals generated by a single laser pulse, since the spectral characteristics of the PA signals are determined by the optical absorption properties of the medium [25].

2. Materials and methods

2.1 Experimental setup

The experimental setup used to test the all-optical US/PA imaging scanhead is shown in Fig. 1(a). The imaging scanhead, which is based on optical US/PA generation and detection, consisted of an optical fiber with an axicon tip for light illumination, and a polymer microring resonator for acoustic detection of both US and PA signals. Optical beam splitting was necessary so that US imaging and PA imaging could be performed with a single laser pulse; this was achieved with the axicon tip. As shown in Figs. 1(b) and 1(c), one portion of the laser energy was applied to the substrate (silicon wafer) of the microring device to induce an acoustic signal for US transmission (Fig. 1(b)), while the other part of the laser pulse illuminated the sample directly for PA imaging (Fig. 1(c)). The total energy at the axicon fiber tip is 2 mJ/pulse. Determined by the geometry, only a fraction of the laser energy is irradiated on the substrate for ultrasound generation. The acoustic pressure measured by the hydrophone is about 102 kPa at a distance of 1 cm away from the optical absorbing substrate. The center frequency is 15 MHz with −6 dB bandwidth of 28 MHz. The microring resonator was fabricated using nanoimprint lithography, and consisted of a 100-μm-diameter polystyrene ring waveguide closely coupled to a bend-back bus waveguide. The microring had a diameter of 95 μm. The waveguide was 2.4 μm wide and 1.85 μm high. The width of the whole microring device was 3.5 mm. The photography and a schematic diagram are shown in Figs. 1(d) and 1(e). The input ðber was connected to a continuous-wave tunable laser source (TSL-510, Santec, Japan), and the output ðber was connected to a high-speed photodetector (1811-FC, New Focus, San Jose, CA) with a gain of 4×10^4 V/A and an electrical bandwidth of DC to 125 MHz. The other laser in the system was a tunable Ti:sapphire pulsed laser (CF-125, SOLAR TII, Minsk, Republic of Belarus) pumped by a Nd:YAG laser (TII LS-2137, LOTIS, Minsk, Belarus) with a 10-Hz repetition rate. The laser energy used to generate US and PA signals was coupled into a high-numerical-aperture (0.22 NA) multimode optical fiber (Thorlabs, Newton, NJ) using a focusing lens. This configuration resulted in a single laser pulse generating US and PA signals simultaneously, with both signals being received by the microring. The signals were digitized with a 200-Msamples/s A/D converter (CompuScope 14200, Gage, Lachine, QC, Canada) and postprocessed on a PC.

#158690 - $15.00 USD Received 23 Nov 2011; revised 28 Dec 2011; accepted 28 Dec 2011; published 10 Jan 2012

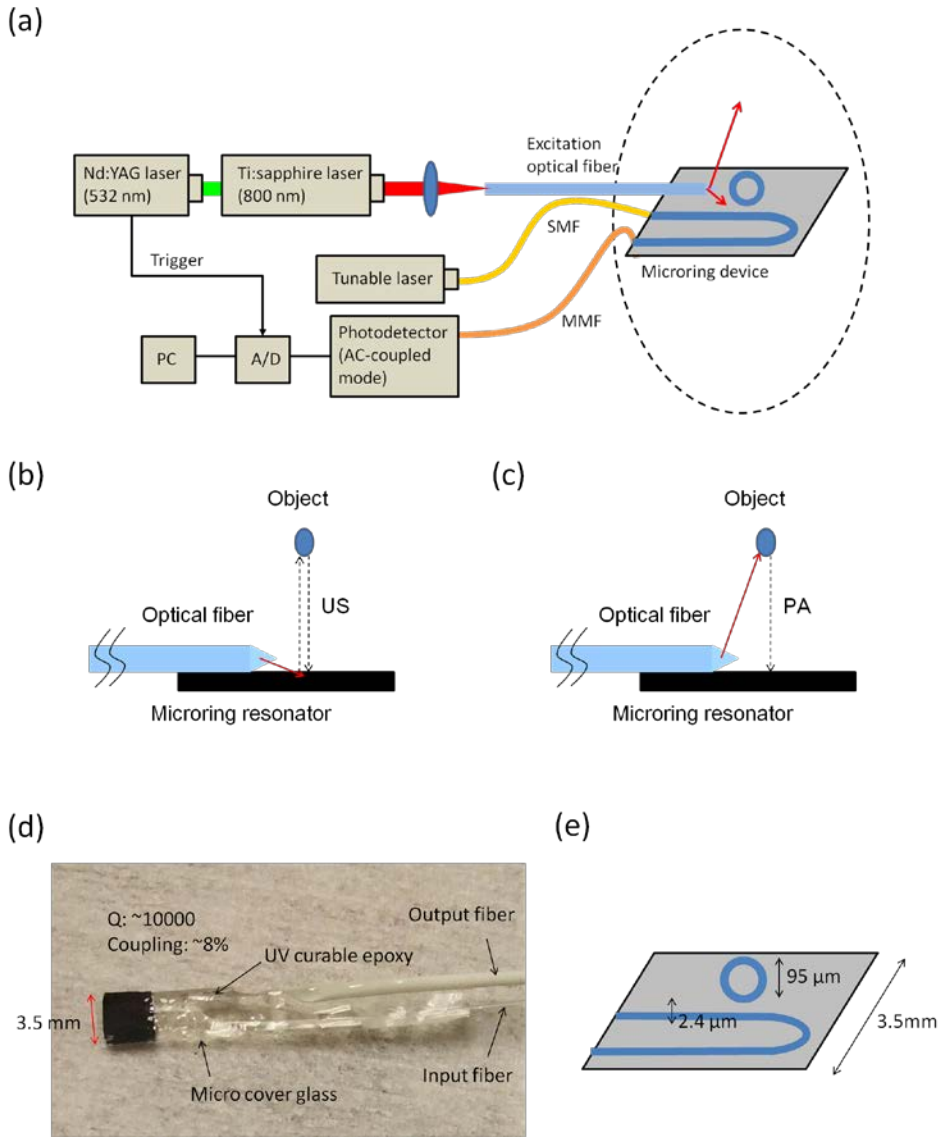

Fig. 1. (a) Experimental setup of the all-optical US/PA imaging system, the mechanisms of US imaging (b) and PA imaging (c), photograph (d) and schematic diagram (e) of the microring device. SMF, single-mode fiber; MMF, multimode fiber.

2.2 Imaging-resolution measurement

The spatial resolution of the imaging system was determined by linearly scanning a strand of hair with a diameter of 100 μm at a step size of 0.1 mm. Signals were acquired using the all-optical imaging scanhead and then processed through the back-projection algorithm to achieve receive focusing [26].

2.3 Grid-phantom study

US and PA images of a grid phantom were also acquired using the same imaging method to further demonstrate the capabilities of the scanhead. The grid phantom comprised a carbon-black grid pattern printed on a thin plastic film (Fig. 2). The lines had a width of 0.9 mm and a

#158690 - $15.00 USD Received 23 Nov 2011; revised 28 Dec 2011; accepted 28 Dec 2011; published 10 Jan 2012

spacing of 2.5 mm. The grid phantom was scanned by the C-scan format to acquire US and PA 3-D information.

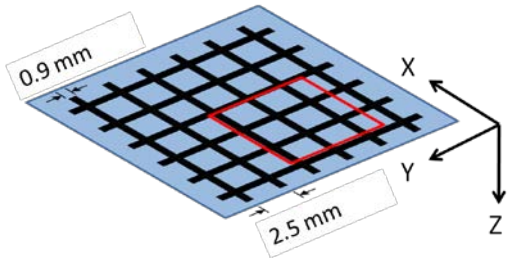

Fig. 2. Configuration of the grid phantom. (the red rectangle indicates the scanning area).

2.4 Subband imaging for further separation of US/PA signals

When the image object is located within a small depth range, the pulse-echo US and PA signals can be separated based on their different propagation delays (i.e., involving a round trip and a one-way trip, respectively). However, when the image object is larger in depth, these two signals overlap. For this case we propose adopting the subband imaging method to separate the US and PA signals [25]. This method is based on the different spectral characteristics of PA signals generated by objects with different absorption properties. Therefore, the contrast between the two signals can be enhanced by applying appropriate bandpass (BP) filtering and postprocessing. The selection of suitable BP filters requires prior knowledge of the frequency responses of the PA signals generated by the different materials. In this study the PA signals generated by the carbon grid pattern on the transparent thin film and the silicon wafer were measured by a 20-MHz piezoelectric transducer with backward-mode setup. Except for the transducer, all other settings were the same as those for all-optical measurements. Based on the frequency responses of these two signals, a higher 20–23MHz BP filter was selected for the PA signals. On the other hand, a lower 12–15MHz BP filter was used for the US signals. The US and PA images are inherently co-registered. The filter design is shown in Fig. 3.

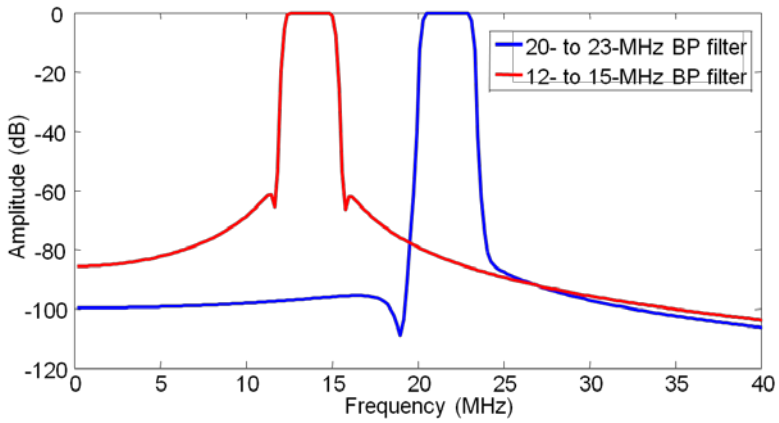

Fig. 3. Frequency responses of the two BP filters for subband imaging.

3. Results

3.1 Spatial-resolution measurements

Images of the hair phantom before and after applying a back-projection reconstruction algorithm [21] are shown in Fig. 4. The imaging resolution is poor in Fig. 4(a) due to the wide

#158690 - $15.00 USD Received 23 Nov 2011; revised 28 Dec 2011; accepted 28 Dec 2011; published 10 Jan 2012

detection angle of the microring resonator and lack of focusing. Back-projection reconstruction (i.e., focusing) improved the—6 dB resolution to 305 and 169 μm in the lateral and axial directions, respectively, as shown in Fig. 4(b).

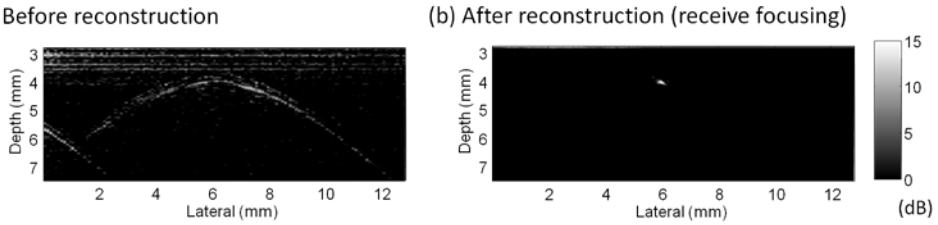

Fig. 4. Hair-phantom images before (a) and after (b) reconstruction.

3.2 Grid phantom

The C-scan image of the grid phantom shown in Fig. 5 indicates that both the US echoes from the thin plastic film and the PA signals generated by the black grid pattern were detected. The different time delays of these two signals made it possible to separate them in the temporal (or depth) direction. The US image provided structure and location information about the thin plastic film, while the PA image revealed the grid pattern thereon. These two images could be co-registered and displayed as a fusion image.

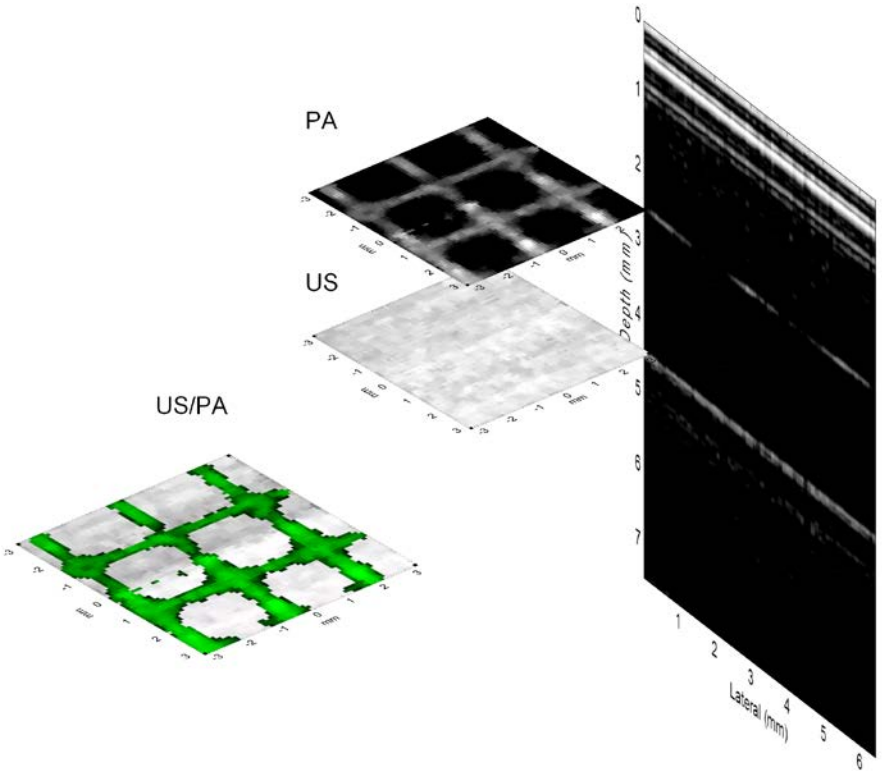

Fig. 5. US, PA, and fusion images of the grid phantom.

#158690 - $15.00 USD Received 23 Nov 2011; revised 28 Dec 2011; accepted 28 Dec 2011; published 10 Jan 2012

3.3 US/PA signal separation

The PA measurements indicated that the absorption coefficient of the grid pattern was larger than that of the silicon wafer, and so the spectrum of the PA signals contained more high-frequency components. This result was consistent with previous simulations and experimental results [20], and indicates that a higher absorption coefficient results in the presence of higher frequency components in the spectrum. Based on the different frequency responses of the PA signals generated by these two materials (see Fig. 6), two BP filters (with passbands of 20–23 MHz and 12–15 MHz) could be applied to further enhance the contrast between the US and PA signals. Figure 7 shows that the contrast of US signals was enhanced by 6 dB by applying BP filtering from 12 to 15 MHz (Fig. 7(b)), and that of the PA signals was enhanced by 5 dB by filtering from 20 to 23 MHz (Fig. 7(c)). Finally, Fig. 7(d) shows the fusion image of the enhanced US and PA images, which shows the combined acoustic and optical absorption information.

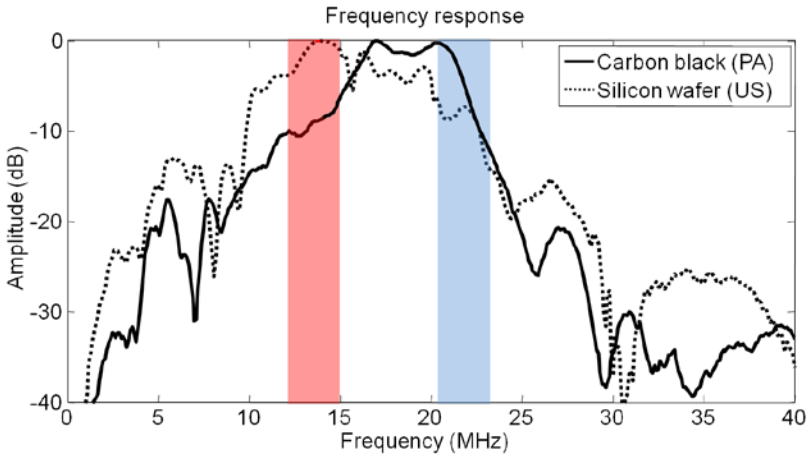

Fig. 6. PA frequency responses of the carbon black and silicon wafer. Red shading, 12- to 15-MHz BP filter; blue shading, 20- to 23-MHz BP filter.

#158690 - $15.00 USD Received 23 Nov 2011; revised 28 Dec 2011; accepted 28 Dec 2011; published 10 Jan 2012

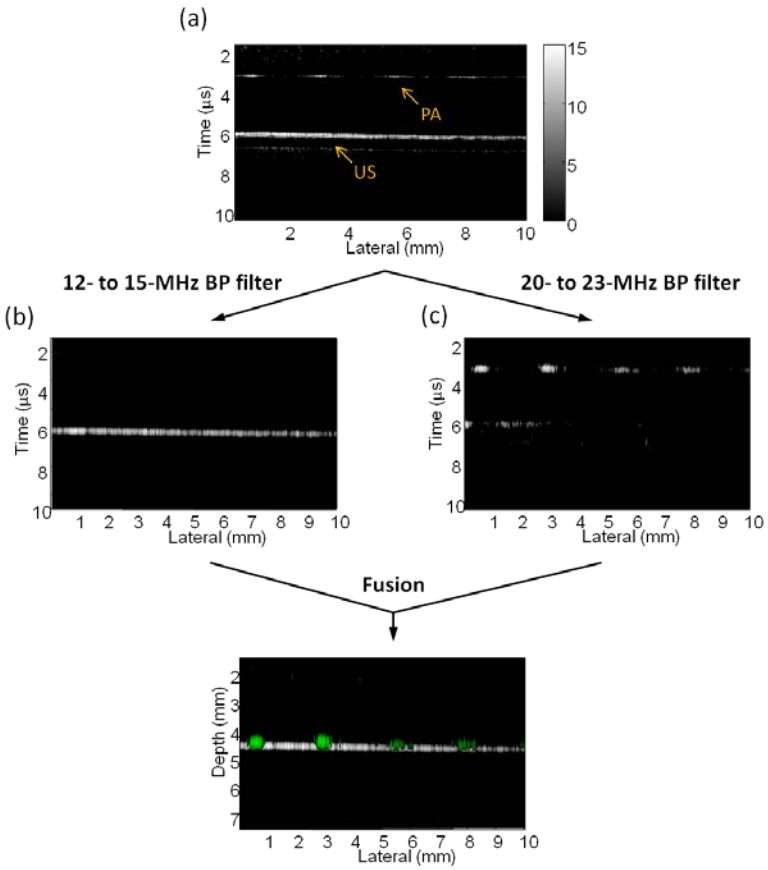

Fig. 7. (a) Original image, (b) enhanced US image obtained by the 12- to 15-MHz BP filter, (c) enhanced PA image obtained by the 20- to 23-MHz BP filter, and (d) fusion image.

4. Discussion

In our all-optical design, US and PA signals can be acquired with a single laser pulse, but the challenge is to separate US and PA signals. Our results demonstrate that the subband imaging technique is effective in separating US and PA signals if the absorption spectra have significant difference between the US-generating material (US imaging) and the image object (PA imaging). It can be used both for nondestructive testing and biomedical applications. The thin film for US generation should be selected based on the optical absorption properties of the image object of interest. The BP frequency bands for subband imaging should be selected based on spectra of the US and the PA signals and the performance can be improved by optimal weighting [25]. Nonetheless, it is necessary to measure the US and PA spectra in advance. One of the potential applications of such a technique is PA contrast imaging, where the exogenous contrast agent can have distinct absorption properties from the substrate and generate ultrasound in a distinctly different frequency band. Certainly, if the spectra are not very separable, performance of this technique is limited.

Smaller piezoelectric transducers inherently exhibit lower sensitivity. In contrast, there is no trade-off between the size and sensitivity of elements for a microring device, which means that it has a sensitivity advantage over conventional piezoelectric transducers when small devices are required. The described all-optical technique can simplify configuration of the scanhead and reduce the cost because no electronic components and conventional piezoelectric materials are needed. In addition, the microring detectors can be fabricated using a nanoimprint technique, which makes mass production possible.

#158690 - $15.00 USD Received 23 Nov 2011; revised 28 Dec 2011; accepted 28 Dec 2011; published 10 Jan 2012

In this study, the acoustic pressure generated by our device is about 102 kPa. The center frequency is 15 MHz with a −6 dB bandwidth of 28 MHz. In the literature, Y. Hou et al. developed the first all-optical US transducer by combining optical generation and detection of US [14]. According to this work, it is possible to generate higher acoustic pressure for US transmission because the specific optical absorbing material in their design has higher thermoexpansion coefficient. Likewise, it is also possible to generate US signals with a higher center frequency and larger bandwidth. The purpose of our study, on the other hand, is to present a pioneering study of an all-optical US/PA imaging scanhead. The future works include optimizing the absorbing thin film for higher acoustic pressure output, higher center frequency and wider bandwidth during US generation. It will also be valuable to expand the single element to an array. We believed that this design has the potential to produce a miniature and cost-effective array transducer for use in endoscopic and intravascular imaging applications.

5. Conclusions

We have demonstrated the capabilities of a newly designed all-optical US/PA imaging scanhead using phantom data. US and PA imaging can be performed within a single laser pulse, and both kinds of signals can be detected using the same microring resonator. Both US and optical contrast information can be acquired by the all-optical imaging scanhead. Moreover, the contrast between the US and PA signals can be increased by using subband imaging.

Acknowledgments

Financial support from the National Science Council and the NTU Center for Advanced Nano-Materials is greatly appreciated.

#158690 - $15.00 USD Received 23 Nov 2011; revised 28 Dec 2011; accepted 28 Dec 2011; published 10 Jan 2012